Direct-Dynamics Study of the F + CH_4, C_2H_6, C_3H_8, and *i*-C_4H_{10} Reactions†

Joshua P. Layfield, Andrew F. Sweeney, and Diego Troya*

Department of Chemistry, Virginia Tech, 107 Davidson Hall, Blacksburg, Virginia 24061-0212

Received: December 11, 2008; Revised Manuscript Received: February 6, 2009

We present a theoretical study of the dynamics of the first few members of the F + alkane → HF + alkyl family of reactions (alkane = CH_4, C_2H_6, C_3H_8, and *i*-C_4H_{10}). Quasiclassical trajectories have been propagated employing a reparameterized semiempirical Hamiltonian that was derived in this work based on ab initio information of the global potential-energy surfaces of all reactions studied. The accuracy of the Hamiltonian is probed via comparison of the calculated dynamics properties with experimental results in the F + CH_4 → HF + CH_3, F + CD_4 → DF + CD_3, and F + C_2H_6 → HF + C_2H_5 reactions. Additional calculations on the F + C_3H_8 → HF + C_3H_7 and F + *i*-C_4H_{10} → HF + C_4H_9 reactions have been analyzed with emphasis on the difference in the dynamics of reactions occurring at primary, secondary, and tertiary sites. We learn that at low collision energies, the amount of energy going into HF vibration increases very slightly along the primary → secondary → tertiary sequence. In addition, reactions involving larger alkane molecules tend to channel more energy toward alkyl products at the expense of the rest of the degrees of freedom. Angular distributions are also dependent on the abstraction site, with tertiary abstractions resulting in slightly more backward scattering than reactions at primary sites.

I. Introduction

Recent measurements of the dynamics of atomic-radical + alkane reactions are continuing to instigate the development of theoretical reaction-dynamics studies that complement the descriptions that experiment can provide.[1−7] Use of full-dimensional quantum-dynamics techniques coupled with highly accurate analytic potential-energy surfaces has enabled impressive agreement between experimental results and theoretical predictions for various triatomic systems,[8,9] but progress to larger reactions has been slow. The ability to move from triatomic reactions to higher dimensionality systems, such as radical + alkane reactions, is difficult due to two main limiting factors. First, a full quantum-dynamics treatment of multidimensional chemical reactions is currently unwieldy. Second, despite promising advances,[10,11] approaches to obtain analytical potential-energy surfaces for polyatomic reactions in a timely manner are still scarce.

Accurate potential-energy surfaces are required to enable quantitative description of the dynamics of chemical reactions by theoretical means. Construction of these potential-energy surfaces has traditionally been carried out by fitting analytic functions to high-quality ab initio data. However, physically reasonable behavior in regions of the global potential-energy surface not covered by the ab initio data cannot always be guaranteed in this approach, and this becomes an issue for systems having many degrees of freedom, such as radical + alkane reactions. A way to circumvent the need for an explicit potential-energy surface is the use of direct dynamics.[12] Direct-dynamics studies calculate the necessary information about the potential-energy surface using electronic-structure methods whenever they are required in the dynamics simulation. A disadvantage of this method is that a typical reaction-dynamics study with classical trajectories can require an excess of 10^7 energy and gradient calculations, which dramatically confines the types of electronic-structure methods that can be used in all but the simplest reactions. This limitation restricts the overall accuracy of the studies and represents a major hurdle for the use of direct dynamics.

Semiempirical Hamiltonians have emerged as a promising class of electronic-structure methods for timely computation of the myriad of potential energies and gradients involved in a direct-dynamics study. These computationally inexpensive methods are a simplification of the Hartree−Fock theory based on neglect of three- and four-centered integrals, parametrization of additional lower order integrals, and use of pseudominimal basis sets, among other approximations.[13] These approximations drastically reduce the computational expense associated with ab initio and even density-functional theories, making semiempirical Hamiltonians attractive candidates for use in large-scale reaction-dynamics studies. The deficiencies in accuracy resulting from these major simplifications to Hartree−Fock theory are partially compensated by inclusion into the Hamiltonian empirical parameters, which are adjusted using information obtained at a more sophisticated level of theory or from experiment. While the resulting semiempirical Hamiltonians possess impressive accuracy/computational-expense ratios for the systems included in the derivation of the empirical parameters, accuracy outside the calibration set is commonly lacking. This is particularly true in the description of the global potential-energy surfaces of chemical reactions, as situations in which bonds are forming or breaking are typically not included in the calibration sets of popular semiempirical Hamiltonians.

Building a specific-reaction-parameter (SRP) semiempirical Hamiltonian has proven to be a convenient method to overcome the often-large inaccuracies of standard semiempirical methods in describing global potential-energy surfaces of relatively simple chemical reactions.[14−21] SRP Hamiltonians are created by deriving a new set of parameters so that the Hamiltonians describe ab initio or experimental information on the potential-energy surface of only a single reaction as accurately as possible. The improved semiempirical Hamiltonians are then used in

† Part of the "George C. Schatz Festschrift".

* Corresponding author. E-mail: troya@vt.edu.

10.1021/jp810929e CCC: $40.75
Published on Web 03/18/2009

TABLE 1: Reaction Energies for F + Alkane → HF + Alkyl Reactions[a]

reaction	CCSD(T)[b]	MP2[c]	MSINDO	SRP-MSINDO	exptl[d,e]
F + CH_4	−30.09 (−26.63)	−35.24 (−31.78)	−36.59 (−32.70)	−32.10 (−28.21)	−31.4, −31.6
F + C_2H_6	−33.20 (−29.54)	−38.08 (−34.35)	−46.50 (−42.80)	−35.40 (−31.63)	−35.3, −35.8
F + C_3H_8 (1)[f]	−32.81 (−29.28)	−37.50 (−33.99)	−45.88 (−42.68)	−35.95 (−32.25)	−35.2, −35.4
F + C_3H_8 (2)[g]	−35.24 (−31.62)	−39.75 (−36.13)	−53.95 (−50.69)	−38.59 (−34.99)	−38.6, −37.8
F + i-C_4H_{10} (1)[h]	−32.13 (−28.70)	−36.65 (−33.23)	−46.62 (−43.36)	−36.25 (−32.75)	−35.7
F + i-C_4H_{10} (3)[i]	−36.43 (−33.16)	−40.67 (−37.40)	−60.17 (−56.90)	−40.85 (−37.25)	−40.7

[a] Energies are reported in kcal mol^{-1}. Values in parentheses correspond to classical energies, i.e., not corrected by zero-point energies. [b] CCSD(T)/aug-cc-pVDZ//MP2/aug-cc-pVDZ energies. [c] MP2/aug-cc-pVDZ energies. [d] Reference 34. [e] Reference 35. [f] F + C_3H_8 → HF + $CH_2CH_2CH_3$. [g] F + C_3H_8 → HF + CH_3CHCH_3. [h] F + i-C_4H_{10} → HF + $CH_2CH(CH_3)_2$. [i] F + i-C_4H_{10} → HF + $C(CH_3)_3$.

direct-dynamics calculations of the single reaction under consideration, and their accuracy can be further tested by comparison of computed dynamics properties with available experimental results. While this approach has been shown to work reasonably well in a variety of reaction-dynamics studies, one of its limitations is that a SRP Hamiltonian needs to be derived for each specific reaction under study. Very recent efforts have investigated the possibility of deriving SRP Hamiltonians specific to a homologous *family* of reactions, in contradistinction with a *single* reaction. Specifically, our group has recently derived a SRP Hamiltonian to study the H + alkane class of reactions by including ab initio information of the potential-energy surface of the first few members of the family in the derivation of the SRP set of parameters.[22] The resulting Hamiltonian generally reproduces experimental information, including relative excitation functions, alkyl product speed distributions, and angular distributions for the H + methane → H_2 + methyl reaction, and the absolute excitation function of the H + C_2D_6 → H_2 + C_2D_5 reaction. The encouraging results of the SRP Hamiltonian for these two reactions have elicited a study of its applicability to larger reactions in the family.[23]

In this paper, we develop a SRP Hamiltonian for the F + alkane class of reactions and carefully calibrate its accuracy by comparison of calculated dynamics properties in the F + CH_4 → HF + CH_3, F + CD_4 → DF + CD_3, and F + C_2H_6 → HF + C_2H_5 reactions with available experiments. Once the accuracy of the Hamiltonian is determined, we investigate the F + methane, ethane, propane, and isobutane reactions with the goal of learning the effect that the abstraction site in the alkane molecule (i.e., primary vs. secondary vs. tertiary) and alkyl fragment size have on the reaction dynamics. Motivation for these studies is provided in part by the intense activity that has been recently focused on the F + alkane → HF + alkyl family of reactions. The dynamics of the F + CH_4 → HF + CH_3 reaction has been extensively studied due to its significant potential as a chemical laser[24] and for fundamental reasons. Experimental studies have provided CH_3 product energy distributions,[25] HF rovibrational state distributions,[4] relative excitation functions,[26] and angular distributions.[27] Isotopically substituted analogues of the F + CH_4 reaction have also been extensively studied.[1,28,29] Several theoretical reaction-dynamics studies of the F + CH_4 system based on analytical surfaces,[30,31] interpolated surfaces,[32] and a SRP Hamiltonian[20] have emerged recently, providing different levels of agreement with experiment. In stark contrast with the vigorous theoretical studies of the F + CH_4 → HF + CH_3 reaction, analogous studies for the next member of the F + alkane family, F + C_2H_6 → HF + C_2H_5, are lacking, which is likely due to the difficulty in deriving analytic potential-energy surfaces mentioned before. In fact, no direct comparison between calculated vibrational distributions of the HF product arising from a full-dynamics study and those measured by Nesbitt and co-workers[5] has been reported yet, and this provides additional motivation for the present study.

The remainder of this paper is as follows. First, we show ab initio calculations performed to capture the main aspects of the F + alkane potential-energy surfaces. Then we use this information to reparameterize a semiempirical Hamiltonian. We then present a direct-dynamics study where this Hamiltonian is used to propagate trajectories for the F + CH_4, C_2H_6, C_3H_8, and i-C_4H_{10} reactions with a focus on computing experimentally determined properties to test the accuracy of the Hamiltonian and investigating the differences in the dynamics of F + alkane reactions as a function of the reagent alkane molecule.

II. Electronic-Structure Calculations

A. Ab Initio Study. We have characterized the main stationary points of the F + CH_4, C_2H_6, C_3H_8, and i-C_4H_{10} reactions using both ab initio and semiempirical methods. Ab initio geometry optimizations and frequency calculations have been performed for all reactions by using second-order Moller−Plesset perturbation theory (MP2) in combination with Dunning's correlation-consistent double-ζ basis set augmented with diffuse functions (aug-cc-pVDZ). Single-point coupled-cluster calculations with single, double, and pertubative triple excitations [CCSD(T)] with the same basis set have been carried out with the MP2 geometries to obtain a higher accuracy estimate of the energies. The validity of these CCSD(T)//MP2 dual-level calculations in determining reaction energies has been shown before for the F + CH_4 reaction, where "pure" CCSD(T)/aug-cc-pVDZ results agree with CCSD(T)/aug-cc-pVDZ//MP2/aug-cc-pVDZ energies within 0.01 kcal mol^{-1}.[20] All of the ab initio calculations have been performed with the Gaussian03 package of programs.[33] Even though nonadiabatic crossings between the three potential-energy surfaces that correlate with the $^2P_{3/2}$ and $^2P_{1/2}$ states of F are expected, experiments on the effect of nonadiabatic dynamics are still lacking. Therefore, our calculations refer only to the ground state potential-energy surface.

Table 1 shows the calculated energies of the F + alkane reactions studied in this work in comparison with experiment.[34,35] The F + C_3H_8 and F + i-C_4H_{10} reactions each have two possible channels, corresponding to the two possible sites of hydrogen abstraction in each alkane molecule (primary and secondary in C_3H_8 and primary and tertiary in i-C_4H_{10}). Moreover, there are two symmetry-inequivalent primary sites for each of these two reactions at 0 K (see Figures 1 and 2 of ref 36), but the differences in the potential-energy surfaces of these two approaches are so small that we will not distinguish them here. Instead, we report the lowest energy channel for primary abstraction, which for both C_3H_8 and i-C_4H_{10} corresponds to sites that produce $CH_2CH_2CH_3$ and $CH_2CH(CH_3)_2$ radicals of C_1 symmetry.

The CCSD(T)/aug-cc-pVDZ results shown in Table 1 uniformly underestimate the experimental reaction exothermicity beyond the limit of chemical accuracy (∼1 kcal mol^{-1}) for all of the reactions studied. This inability of CCSD(T)/aug-cc-

TABLE 2: Calculated Transition-State Geometric Properties and Reaction Barriers for F + Alkane → HF + Alkyl Reactions[a]

	R(F−H)/Å	R(C−H)/Å	∠F−H−C/deg	energy[b]/kcal mol^{-1}
		MP2/aug-cc-pVDZ		
F + CH_4	1.466	1.137	180.0	1.45 (3.44)
F + C_2H_6	1.545	1.130	161.3	0.15 (1.65)
F + C_3H_8 (1)[c]	1.552	1.131	156.6	−0.02 (1.36)
F + C_3H_8 (2)[d]	1.621	1.125	149.4	−0.58 (0.38)
F + i-C_4H_{10} (1)[e]	1.549	1.130	157.8	−0.08 (1.33)
F + i-C_4H_{10} (3)[f]	1.691	1.122	148.7	−1.00 (−0.39)
		MSINDO		
F + CH_4	1.284	1.131	180.0	2.53 (3.85)
F + C_2H_6	1.400	1.128	165.7	0.97 (1.91)
		SRP-MSINDO		
F + CH_4	1.546	1.117	180.0	0.85 (1.16)

[a] Reactions missing from the table indicate that a transition state could not be located with that particular method. [b] Values in parentheses correspond to classical energies, i.e., not corrected by zero-point energies. [c] F + C_3H_8 → HF + $CH_2CH_2CH_3$. [d] F + C_3H_8 → HF + CH_3CHCH_3. [e] F + i-C_4H_{10} → HF + $CH_2CH(CH_3)_2$. [f] F + i-C_4H_{10} → HF + $C(CH_3)_3$.

pVDZ calculations to capture the reaction energies with chemical accuracy is mainly due to the use of an insufficiently large basis set. In effect, complete-basis-set extrapolations from CCSD(T)/aug-cc-pVTZ and -pVQZ calculations for the F + CH_4 → HF + CH_3 ($\Delta_r H$ = −33.18 kcal mol^{-1}) and F + C_2H_6 → HF + C_2H_5 reaction ($\Delta_r H$ = −36.78 kcal mol^{-1}) provide the level of agreement with experiment expected from CCSD(T) calculations. In contrast to the uniform underestimation of the reaction exothermicities by CCSD(T)/aug-cc-pVDZ calculations, MP2/aug-cc-pVDZ reaction energies are usually more exothermic than experiment for the smaller members of the family, but coincidentally agree with experiment quite well for the F + i-C_4H_{10} reactions.

Table 1 also contains results obtained with the standard MSINDO semiempirical Hamiltonian.[37,38] Remarkably, the reproduction of the reaction energy of the F + CH_4 → HF + CH_3 reaction is comparable to that of MP2/aug-cc-pVDZ calculations, even though the ab initio calculations are orders of magnitude more computationally demanding. However, the ability of MSINDO to be within 3 kcal mol^{-1} of the experimental reaction energy in F + CH_4 quickly disappears when one examines the results for larger F + alkane reactions. For F + C_2H_6, the errors in the MSINDO predictions rise to 10 kcal mol^{-1}, and they continue to escalate for the reaction energies involving secondary and tertiary sites. In fact, the poorest description of the experiment occurs for the abstraction at the tertiary site in the F + i-C_4H_{10} reaction, for which the MSINDO reaction energy is almost 20 kcal mol^{-1} more negative than experiment. Notwithstanding, the expected trend[39] that the reactions become more exothermic in the primary → secondary → tertiary sequence is borne out by all electronic-structure methods, including MSINDO.

Table 2 shows the calculated barriers for the F + alkane reactions studied here and the essential geometric parameters of the corresponding transition states, including the lengths of the forming (F−H) and breaking (C−H) bonds and the angle formed by them. (The absence of values for some of the reactions under the MSINDO calculations means that no first-order transition state was found for those reactions.) The properties of the transition state of the F + CH_4 → HF + CH_4 reaction have been discussed at length in the literature.[20] Briefly, the transition state located at the MP2/aug-cc-pVDZ level has

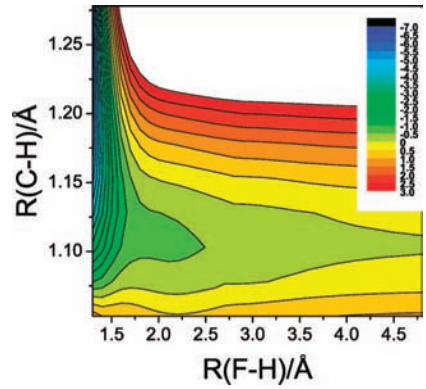

Figure 1. Contour plot of the potential-energy surface of the F + C_2H_6 → HF + C_2H_5 reaction at the CCSD(T)/aug-cc-pVDZ level. F−H is the forming bond and C−H is the breaking bond. These bonds are held collinear in the scans and the rest of the variables are fixed at their values in reagents. Units of the z-axis scale are kcal mol^{-1}.

a much earlier character than the predictions of CCSD(T)/aug-cc-pVDZ (R(F−H) = 1.643 Å, R(C−H) = 1.124 Å, ∠F−H−C = 153.4°, reaction barrier = −0.43(0.32) kcal mol^{-1} [20]). This result limits the usefulness of dual-level CCSD(T)/aug-cc-pVDZ//MP2/aug-cc-pVDZ calculations of the reactions barriers, and therefore such calculations are not shown in Table 2. Two points are worth noting about the transition state of the F + CH_4 → HF + CH_3 reaction predicted by the standard MSINDO semiempirical Hamiltonian. First, it has a much earlier character than MP2. Second, the reaction barrier (3.85 kcal mol^{-1} without inclusion of zero-point energy) is higher than MP2/aug-cc-pVDZ. This result is significant because in the experiments carried out by the Nesbitt group on this reaction, the collision energy is only 1.8 kcal mol^{-1}, which is below the MSINDO classical barrier. Therefore, even though the absolute difference between the MSINDO barrier and more accurate estimates is relatively small, quasiclassical-trajectory studies at the collision energy of the Nesbitt experiment would result in no reactivity unless zero-point energy leakage from the CH_4 molecule to the reaction coordinate occurs. To further investigate the ability of the original MSINDO Hamiltonian to simulate experiment, we integrated 10 000 trajectories at 1.8 kcal mol^{-1} collision energy and found only 4 reactive ones, which emerge from zero-point energy violations along the trajectories. Therefore, even though the deviations between the predictions of the standard MSINDO Hamiltonian and ab initio methods are not dramatic for the F + CH_4 reaction, this method clearly does not provide reliable physical insight into the reaction under experimental conditions.

Examination of the MP2 saddle-point geometries for the various F + alkane reactions in Table 2 shows that the transition state becomes increasingly earlier along the primary → secondary → tertiary sequence. This shift in the geometry of the transition state toward reagents is accompanied by a decrease in the barrier height and an increase in the reaction exothermicity (Table 1). All these results are rubrics of the well-known Hammond postulate,[40] and agree nicely with similar recent work on O + alkane reactions.[36]

CCSD(T)/aug-cc-pVDZ geometry optimizations failed to locate a transition state for the F + C_2H_6 → HF + C_2H_5 reaction. To verify whether this reaction possesses a first-order saddle point at the CCSD(T)/aug-cc-pVDZ level, we show in Figure 1 contour plots of the relevant region of the potential-energy surface calculated at that level of theory. The two-dimensional grid of points has been obtained by scanning the breaking and forming bonds in a collinear geometry while holding the rest

of the coordinates of the system fixed at their values in reagents. The fact that the F−H and C−H bonds are collinear and the ethyl moiety is not allowed to relax during the scans will result in an increase in the potential energy with respect to the true minimum-energy reaction path. Figure 1 shows that even though the calculated scans do not truly represent the minimum-energy reaction path, the pathway from reagents to products is continuously downhill at the CCSD(T)/aug-cc-pVDZ level, confirming the absence of a first-order transition state. On the basis of Hammond's postulate, we do not anticipate that the larger reactions will exhibit transition states at the CCSD(T)/aug-cc-pVDZ level, particularly for the more exothermic secondary and tertiary reaction channels.

B. SRP-MSINDO Hamiltonian. As stated earlier, a computationally inexpensive method to calculate the potential energy and energy gradients of the system is essential for extensive direct-dynamics studies of all but the smallest chemical reactions. Semiempirical methods offer this attractive feature, but as shown in the prior section, do not generally provide sufficient accuracy to achieve meaningful results. For instance, the MSINDO Hamiltonian overestimates the exothermicity of the F + alkane reactions other than F + CH_4 by at least 10 kcal mol^{-1}. Additionally, the errors in the difference in reaction energies between primary and secondary sites in propane (∼8 kcal mol^{-1} for MSINDO and ∼3 kcal mol^{-1} experimentally) and primary and tertiary sites for F + i-C_4H_{10} (∼15 kcal mol^{-1} for MSINDO and ∼5 kcal mol^{-1} experimentally) would likely result in inaccurate conclusions when comparing the dynamics of the reactions at the various sites.

With the goal of obtaining more meaningful results in direct-dynamics studies of F + alkane reactions, we have derived a SRP-MSINDO Hamiltonian specific to that family of reactions that possesses higher accuracy than the standard Hamiltonian. The parameter set for this Hamiltonian has been derived by using ab initio information of the energetically accessible regions of the F + CH_4 and F + C_2H_6 potential-energy surfaces at the conditions of extant experiments, in addition to the reaction energies of all of the reactions studied here. The ab initio characterization of the potential-energy surface of the F + CH_4 → F + CH_3 reaction was carried out via scans of the breaking and forming bonds in a collinear geometry. The forming H−F bond distance was scanned from its value at the MP2/aug-cc-pVDZ transition state (1.46 Å) to 3.96 Å at 0.05 Å steps. During this scan, the F−H−C atoms are forced to be collinear, but the remaining degrees of freedom are optimized at the MP2/aug-cc-pVDZ level. A similar scan of the potential-energy surface was performed for the breaking C−H bond from its distance at the transition state obtained with the same electronic-structure level (1.14 Å) to 3.64 Å at 0.05 Å steps. To obtain a better coverage of regions of the potential removed from the collinear approach and incorporate important points of relatively high energy, we scanned the angle between the forming H−F and breaking C−H bonds from 180° (value of the angle at the transition state in MP2/aug-cc-pVDZ calculations) to 90.0° with steps of 1.0°. In this scan, the H−F and C−H coordinates were held fixed at their transition-state values, but the rest of the coordinates were relaxed at the MP2/aug-cc-pVDZ level. A similar ab initio characterization of the potential-energy surface of the F + C_2H_6 → HF + C_2H_5 reaction was performed, including a scan of the H−F bond from the transition state (1.54 Å) to 5.24 Å at 0.05 Å steps and a scan of the C−H bond from the transition state (1.13 Å) to 4.83 Å with the same step size. In all of the F + C_2H_6 potential-energy scans, the forming and breaking bonds were constrained to the corresponding angle at the transition state (161.3°), but the C_2H_5 moiety was relaxed at the MP2/aug-cc-pVDZ level. Since the MP2/aug-cc-pVDZ level of theory does not provide a highly accurate description of the F + alkane reaction energetics, we have recalculated the energy of each of the points of the MP2/aug-cc-pVDZ scans at the CCSD(T)/aug-cc-pVDZ level.

TABLE 3: List of MSINDO and SRP-MSINDO Parameters That Were Involved in the SRP Development[a]

parameter	MSINDO	SRP-MSINDO
ζ_s^U (H)	1.006	1.11357
ζ_s (H)	1.1576	1.0749
K_s (H)	0.1449	0.1713
I_s (H)	−0.5000	−0.4841
ζ_s^U (C)	1.6266	1.2780
ζ_p^U (C)	1.5572	1.6829
ζ_s (C)	1.7874	2.2545
ζ_p (C)	1.677	1.6671
K_s (C)	0.0867	0.09632
τ_{1s} (C)	5.083	5.1193
ε_{1s} (C)	10.43	10.6686
I_s (C)	−0.8195	−0.7793
I_p (C)	−0.3824	−0.3872
ζ_s^U (F)	2.3408	2.1754
ζ_p^U (F)	2.2465	2.2079
ζ_s (F)	2.4974	2.8586
ζ_p (F)	2.351	2.4626
K_s (F)	0.1769	0.1602
τ_{1s} (F)	8.6043	8.6438
ε_{1s} (F)	25.19	28.2496
I_s (F)	−2.0238	−2.4281
I_p (F)	−0.6868	−0.7015
α(1) (H)	0.3856	0.3811
α(2) (H)	0.5038	0.3432
α(1) (C)	0.4936	0.5465
α(2) (C)	0.6776	0.3410
α(1) (F)	0.1521	0.1489
α(2) (F)	0.1059	0.0031

[a] For a definition of parameters, please see ref 37.

Preliminary reparametrization efforts with the CCSD(T)/aug-cc-pVDZ energies of the 5 scans described before resulted in rather inaccurate H−F and C−C equilibrium bond distances. To avoid those deficiencies, we subsequently included in the ab initio grid a scan of the HF molecule internuclear distance from 0.735 Å to 1.275 Å and a scan of the C−C bond in ethane from 1.430 Å to 1.620 Å. Both scans used a 0.010 Å step size. The grid of ab initio information used for the reparametrization of the MSINDO Hamiltonian also contained the reaction energies of all of the reactions in Table 1. Starting with the parameters of the F, H, and C atoms in the standard MSINDO Hamiltonian, we used a nonlinear least-squares procedure to obtain a new set of parameters for which the differences between the CCSD(T)/aug-cc-pVDZ energies of the points in the grid described before and semiempirical energies were minimum. The parameters were not constrained at any point during the procedure. After several initial attempts, it was determined that attributing different weights to various points of the ab initio grid resulted in an overall better fit. Thus, the final set of SRP parameters was obtained by weighting the points of the entrance channel of the F + CH_4 reaction and the exit channel of the F + C_2H_6 reaction 10 times more heavily than the rest of the points. The SRP parameters obtained in this way are shown in comparison with the original MSINDO parameters in Table 3. The relative differences between the original parameters and the new SRP-MSINDO parameters are on

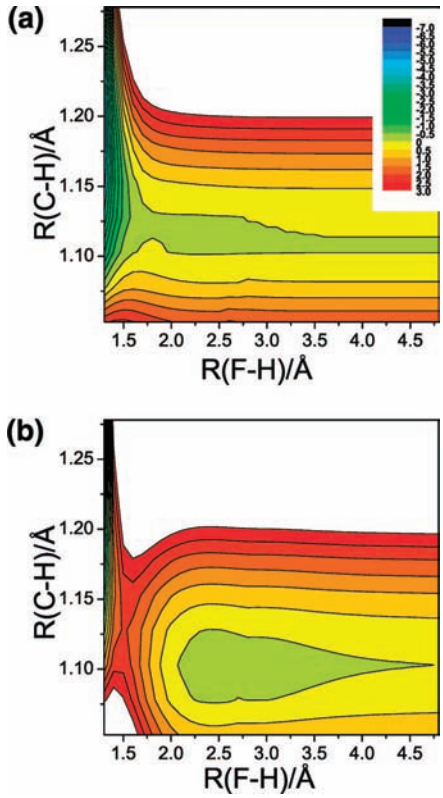

Figure 2. Contour plot of the potential-energy surface of the F + C_2H_6 → HF + C_2H_5 reaction at the SRP-MSINDO (a) and MP2/aug-cc-pVDZ (b) levels. F−H is the forming bond and C−H is the breaking bond. These bonds are held collinear in the scans and the rest of the variables are fixed at their values in reagents. The scale of the *z*-axis (potential energy) is the same as in Figure 1.

average 14%, with only one of the 28 parameters varying by more than a factor of 2.

The improvement in the accuracy of the MSINDO Hamiltonian when using the set of parameters derived here for the F + alkane reactions can be clearly seen in Tables 1 and 2. Table 1 shows that while the original MSINDO Hamiltonian grossly overestimates the CCSD(T)/aug-cc-pVDZ energy of many of the F + alkane reactions studied here, the SRP Hamiltonian is in substantially better agreement, exhibiting an accuracy comparable to that of MP2/aug-cc-pVDZ. Remarkably, the large errors in the differences between the reaction energies of primary and secondary, and primary and tertiary sites obtained with the MSINDO Hamiltonian are nicely corrected in the SRP-MSINDO Hamiltonian. Regarding the transition state locations and energies, SRP-MSINDO also exhibits better agreement with the CCSD(T)/aug-cc-pVDZ results than the original MSINDO Hamiltonian or even MP2/aug-cc-pVDZ results. Notably, the SRP-MSINDO F−H bond distance is 6% shorter than the CCSD(T)/aug-cc-pVDZ result, which is roughly half the deviation of the MP2/aug-cc-pVDZ result. Moreover, the SRP-MSINDO Hamiltonian does not exhibit a barrier for the F + C_2H_6 reaction, which is in agreement with the CCSD(T)/aug-cc-pVDZ predictions (Figure 1). This can be verified in Figure 2a, where we show a contour plot of SRP-MSINDO energies for the same region of the potential-energy surface of the F + C_2H_6 reaction as that displayed in Figure 1 with CCSD(T)/aug-cc-pVDZ energies. In contrast with the absence of a barrier on the classical potential-energy surface predicted by both CCSD(T)/aug-cc-pVDZ and SRP-MSINDO, the contour plot for MP2/aug-cc-pVDZ (Figure 2b) clearly shows a transition state for

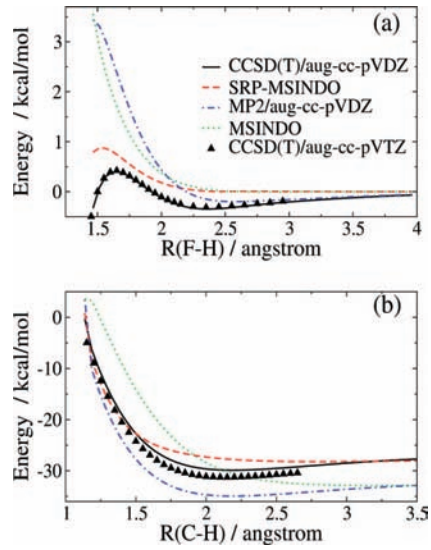

Figure 3. Potential-energy surface profiles of the F + CH_4 → HF + CH_3 reaction calculated at various levels of theory: (a) for the region of the potential-energy surface connecting the transition state with reagents and (b) for the region connecting the transition state with products.

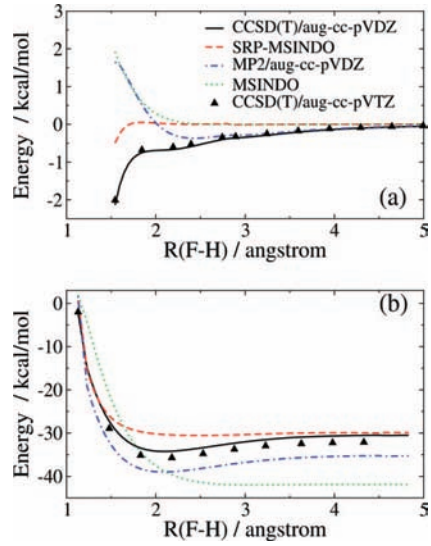

Figure 4. Potential-energy surface profiles of the F + C_2H_6 → HF + C_2H_6 reaction calculated at various levels of theory: (a) for the region of the potential-energy surface connecting the transition state with reagents and (b) for the region connecting the transition state with products.

this collinear approach in which the geometry of the inactive C_2H_5 moiety is fixed to its geometry in reagents.

A more complete calibration of the accuracy of the SRP-MSINDO Hamiltonian with respect to the CCSD(T)/aug-cc-pVDZ results that we have used as a benchmark is presented in Figures 3 and 4. Figure 3 displays the F−H and C−H scans for the F + CH_4 → HF + CH_3 reaction that have been used in the reoptimization of the MSINDO Hamiltonian parameters as described before. Figure 3a shows the region of the potential-energy surface connecting the transition state with reagents. The SRP-MSINDO results deviate from the more accurate CCSD(T)/aug-cc-pVDZ values uniformly by about 0.5 kcal mol^{-1}, and they considerably improve upon the MP2/aug-cc-pVDZ energies. A deficiency of the SRP-MSINDO Hamiltonian is that it is unable to describe the van der Waals' well in the reagents valley predicted by the CCSD(T)/aug-cc-pVDZ method. This

well is caused by dispersion interactions between the approaching reagent species, which are known to be difficult to model by all but the most sophisticated treatments of electron correlation. Even though SRP-MSINDO does not capture the well region with excellent accuracy, it represents a great improvement over a previously published SRP-PM3 Hamiltonian.[20] That Hamiltonian exhibited a sharp, deep well in the region of the potential-energy surface preceding the transition state. This well did not appear to affect classical-trajectory calculations at low energies; however, the appearance of that spurious well in the SRP-PM3 Hamiltonian points out the necessity of providing a dense coverage of ab initio information when deriving SRP Hamiltonians.

Figure 3b shows the region of the F + CH_4 → HF + CH_3 potential-energy surface (PES) connecting the transition state with products. All of the methods predict a precipitous fall in the potential energy with small increases in the C−H coordinate right after the transition state. Much as in the reagents region, while SRP-MSINDO is quite close to the CCSD(T)/aug-cc-pVDZ energies, the agreement is not quantitative. Notably, SRP-MSINDO is unable to describe the well caused by dipole/quadrupole electronic interactions between the separating HF and CH_3 species in the products valley.

Comparisons between similar potential-energy profiles predicted by various electronic-structure methods for the F + C_2H_6 → HF + C_2H_5 reaction are shown in Figure 4. The overall conclusions about the accuracy of the SRP-MSINDO Hamiltonian stemming from the figure are analogous to those mentioned above for the F + CH_4 → HF + CH_3 reaction. SRP-MSINDO reproduces CCSD(T)/aug-cc-pVDZ energies with better accuracy than MP2/aug-cc-pVDZ, except for the shallow potential-energy wells in the reagents and products valleys. Figures 3 and 4 also include CCSD(T) points calculated with the larger aug-cc-pVTZ basis set in an attempt to calibrate the error of the SRP Hamiltonian emerging from having used the relatively small aug-cc-pVDZ basis set in the CCSD(T) calculations used in the fit. Interestingly, use of the aug-cc-pVTZ basis set does not have a dramatic impact on the CCSD(T) energies in reagents, as shown in Figures 3a and 4a. In products, use of the larger basis set results in a slightly more exothermic energy profile. For instance the F + CH_4 → HF + CH_3 reaction is predicted by CCSD(T)/aug-cc-pVTZ calculations to be 1.3 kcal mol^{-1} more exothermic than by CCSD(T)/aug-cc-pVDZ. For the F + C_2H_6 → HF + C_2H_5 reaction, the difference between the aug-cc-pVDZ and -TZ exothermicities increases to 1.7 kcal mol^{-1}. These basis-set studies give a measure of the limits of the accuracy of the SRP MSINDO Hamiltonian stemming from the limited accuracy of the CCSD(T)/aug-cc-pVDZ calibration data points.

Figures 3 and 4 show the performance of the SRP-MSINDO Hamiltonian in the chemical reactions for which ab initio information was explicitly included in the reparametrization. A test of the idea that SRP Hamiltonians can be derived for families of reactions without the need to include ab initio information for all the members of the family can therefore be provided by examining a comparison between CCSD(T)/aug-cc-pVDZ scans for the F + C_3H_8 and F + i-C_4H_{10} reactions and the corresponding SRP-MSINDO energies. This is what we show in Figure 5 for the regions of potential-energy surface connecting the transition state with products for the F + C_3H_8 → HF + CH_3CHCH_3 (Figure 5a) and F + i-C_4H_{10} → HF + $C(CH_3)_3$ (Figure 5b) reactions. We choose to show the profiles of the abstractions at the secondary and tertiary sites in these larger reactions because explicit information about these abstraction channels other than the reaction energies was not included in the SRP optimization, and this therefore poses a more demanding test than the primary channels. The conclusion from Figure 5 is that the SRP Hamiltonian for F + alkane reactions derived in this work by using detailed ab initio information of only the first two members of the family appears to capture larger reactions of the family with comparable accuracy. This conclusion is particularly important, as it offers a practical way to derive improved semiempirical Hamiltonians for a variety of large-dimensionality chemical reactions with minimal high-level ab initio characterization of their PES.

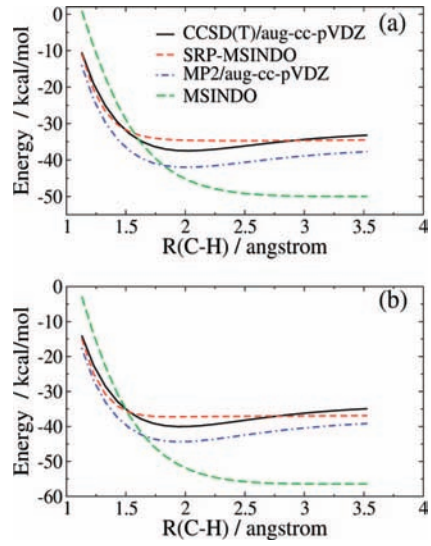

Figure 5. Profiles of the region of the potential-energy surface connecting the transition state with products for the F + C_3H_8 → HF + CH_3CHCH_3 (a) and F + i-C_4H_{10} → HF + t-C_4H_9 (b) reactions calculated at various levels of theory.

III. Direct-Dynamics Study

Using the SRP-MSINDO Hamiltonian derived in this work, we have integrated direct quasiclassical trajectories of the F + CH_4, C_2H_6, C_3H_8, and i-C_4H_{10} reactions. Batches of 20 000 trajectories were calculated for each system and set of initial conditions except for systems and conditions where experimental information exists, for which we raised the number of trajectories to 50 000. The trajectories have been started with the F atom at a distance of 15 au from the center of mass of the hydrocarbon molecule and stopped when the products are ∼15 au apart. The maximum sampling impact parameters are 7.0 au for F + CH_4, and 10 au for F + C_2H_6, F + C_3H_8, and F + i-C_4H_{10} reactions. Initial conditions for the hydrocarbon reagent molecules consider initial zero-point energy and no rotation, and were selected by using the VENUS program.[41] The MSINDO Hamiltonian is known to overestimate vibrational frequencies by ∼20%,[18,22] so we have used VENUS to select initial coordinates and momenta that correspond to 80% of the MSINDO zero-point energy in each of the normal modes. This procedure gives the alkane molecules zero-point energy that corresponds to the experimental values.

From analysis of the atomic initial and final coordinates and momenta, we have calculated a variety of dynamics properties, including partitioning of energy in products, angular distributions, and opacity functions. We first show comparisons with experiment with the goal of calibrating the accuracy of the SRP-MSINDO method for dynamics calculations and subsequently present the results of a comparative study of the dynamics of the various F + alkane reactions studied in this work.

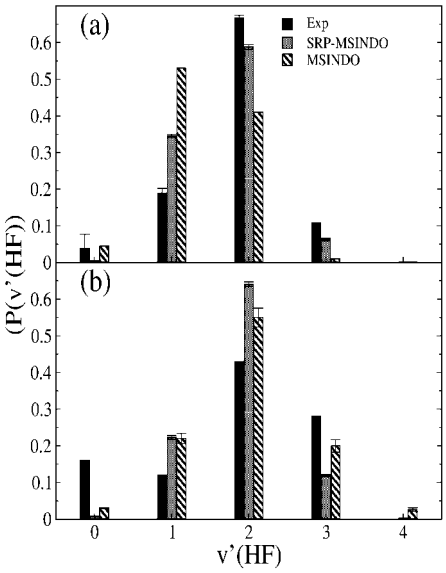

Figure 6. HF vibrational state distribution for the $F + CH_4 \rightarrow HF + CH_3$ reaction at E_{coll}=1.8 kcal mol^{-1} (a) and the $F + C_2H_6 \rightarrow HF + C_2H_5$ reaction at E_{coll} = 3.2 kcal mol^{-1}. The experimental results in part a are taken from ref 4 and those in part b from ref 5. The collision energy in part a for the MSINDO results is 3.2 kcal mol^{-1} (see text).

A. Comparison with Experiments. Figure 6 shows the HF vibrational distributions arising in the $F + CH_4 \rightarrow HF + CH_3$ (Figure 6a) and $F + C_2H_6 \rightarrow HF + C_2H_5$ (Figure 6b) reactions at 1.8 and 3.2 kcal mol^{-1} collision energy (E_{coll}), respectively. The HF vibrational distributions of the $F + CH_4$ reaction show agreement between SRP-MSINDO and the experimental results of Nesbitt and co-workers,[4] with both distributions being clearly inverted and peaking at $v' = 2$. Quantitatively, the average HF vibrational energy (including zero-point energy) in the SRP-MSINDO calculations is 26.7 ± 0.2 kcal mol^{-1}, while the experimental value is 27.4 kcal mol^{-1}. The figure also shows the results calculated by using quasiclassical trajectories with the original MSINDO Hamiltonian at 3.2 kcal mol^{-1}. This collision energy is slightly larger than the one used in the experimental and SRP-MSINDO calculations because, as previously stated, MSINDO calculations at 1.8 kcal mol^{-1} do not provide significant reactivity due to the high reactive barrier of this method. The energy of 3.2 kcal mol^{-1} represents a collision energy above the barrier in the MSINDO calculations similar to that in experiment. MSINDO clearly underestimates the level of vibrational excitation going into the HF vibration, with the peak of the distributions being at $v' = 1$. Figure 3b shows that the origin of this discrepancy with experiment is due to the incorrect shape of the MSINDO potential-energy surface, and not the reaction exothermicity.

Figure 6b shows the SRP-MSINDO HF vibrational distribution arising from the $F + C_2H_6$ reaction at $E_{coll} = 3.2$ kcal mol^{-1} in comparison to the experiments by the Nesbitt group.[5] To our knowledge, this is the first time that full dynamics calculations have been used to simulate those experiments. While the vibrational distributions do not agree quantitatively, the peak of both distributions still occurs at $v' = 2$, neither shows significant population in $v' = 4$, and the average HF vibrational energies are in reasonable agreement with each other (28.7 ± 0.2 kcal mol^{-1} for SRP-MSINDO and 25.7 kcal mol^{-1} in the experiment, including zero-point energy). The main source of discrepancy between theory and experiment occurs for $v' = 0$, where the experiments report 16% of the population, but our calculations only yield 1%. An intriguing aspect of the experiment is the bimodal nature of the vibrational distributions, with $v' = 1$ showing less population than $v' = 0$ and 2. In the experiments, it was discussed that the presence of a larger alkyl fragment than in the case of the $F + CH_4$ reaction might elicit a second mechanism, in addition to a direct, impulsive release of energy in the onset of product separation, that would channel energy from the "active" F−H−C moiety into the alkyl fragment via intramolecular vibrational redistribution (IVR). This second mechanism would act to exclusively populate the HF(v'=0) state. Even though classical trajectories are known to accelerate the rate of IVR, the presence of the speculated mechanism is not seen in the present calculations, so the intriguing bimodality of the experimental distributions must emerge from errors in the SRP-MSINDO Hamiltonian or in our classical treatment of the nuclear dynamics. To verify that the absence of significant population in HF(v'=0) is not associated with zero-point energy leakage from the C_2H_6 molecule into the newly formed HF bond, we have integrated trajectories in which C_2H_6 is started with only half or a quarter of the zero-point energy. None of these calculations yields significant population in HF(v'=0), suggesting that the inability of the calculations to reproduce the subtle bimodality seen in the experiment might be tied to inaccuracies in the SRP-MSINDO Hamiltonian or quantum effects.

Figure 6b also shows the results for the MSINDO Hamiltonian. Even though the MSINDO calculations seem to be in good agreement with experiment, analysis of the average energy deposited into HF vibration (33.4 kcal mol^{-1}) shows a relatively large (∼7.5 kcal mol^{-1}) overestimation of the experiment (25.7 kcal mol^{-1}). An interesting result is that the HF vibrational distributions obtained with the original MSINDO Hamiltonian in the $F + C_2H_6$ reaction (Figure 6a) appear to be in better agreement with experiment than in the $F + CH_4$ reaction (Figure 6b). However, a detailed analysis suggests that the improvement in the agreement with experiment for the $F + C_2H_6$ reaction is largely fortuitous. As shown in Figure 6a, MSINDO underestimates the amount of vibrational excitation going into HF. This underestimation is fortunately balanced out by the ∼10 kcal mol^{-1} overestimation of the reaction exothermicity in the $F + C_2H_6$ reaction by this method (Table 1) so that the amount of energy going into HF seems to agree better with experiment than in the $F + CH_4$ reaction.

The Liu group has measured additional information about the release of energy into products for the $F + CD_4 \rightarrow DF + CD_3$ reaction, including partition of energy into translation, DF vibration, and DF rotation at various collision energies.[1,42] A particularity of those measurements is that they correspond to specific internal states of the CD_3 product. This detail challenges a quantitative comparison with our quasiclassical-trajectory results, since no exact technique to map coordinates and momenta of polyatomic molecules into vibrational states currently exists. In addition, classical-dynamics calculations suffer from rapid IVR, which further complicates the determination of the exact final quantum state of a polyatomic vibration via projection of final coordinates and momenta into harmonic normal modes.[30] Even though establishing comparisons between quasiclassical-trajectory calculations and the CD_3 state-selected experiments is not possible at a quantitative level, a comparison of the trends can provide further insight into the accuracy of the calculations. The Liu group have provided insight into the dependence of energy partitioning in products with collision energy for the $F + CD_4 \rightarrow DF + CD_3(0000,N\approx4)$ reaction.[42] These state-specific results indicate that the amount of HF rotational energy and relative translational energy of the products

TABLE 4: Calculated Average Energies in Products in the F + CD_4 → DF + CD_3 Reaction[a,b]

E_{coll}/kcal mol^{-1}	$\langle E'_{V(DF)}\rangle$[c]	$\langle E'_{R(DF)}\rangle$	$\langle E'_{T}\rangle$	$\langle E'_{CD3}\rangle$
1.48	25.6 (28.0)	2.7 (3.1)	7.7 (7.6)	13.1 (10.5)
2.77	24.7 (27.5)	3.3 (3.5)	9.0 (8.9)	13.4 (10.5)
5.37	23.1 (26.2)	4.1 (4.2)	12.0 (11.8)	13.5 (10.5)
8.36	21.9 (25.7)	4.9 (4.9)	15.1 (14.6)	14.1 (10.6)

[a] All energies in kcal mol^{-1} [b] Values in parentheses correspond to trajectories in which CD_3 arises with less energy that its nominal zero point energy. [c] Calculated from the bottom of the potential well of DF.

increase with increasing collision energy. On the other hand, HF vibrational excitation decreases with collision energy.

Table 4 presents the calculated results of energy partitioning in products at the same collision energies measured in the experiments. The results include averages over all of the trajectories, and of the trajectories in which CD_3 emerges with less energy than its nominal zero-point energy (values between parentheses). The restriction of the analysis to trajectories with low CD_3 is a rough attempt to represent ground-state CD_3 as measured in the experiment. Regardless of the analysis method, the calculated trends agree with experiment: while DF rotational and relative translational energies increase with collision energy, DF vibrational energy decreases with increasing collision energy. Even though the calculations reproduce the experimental trends, limitations in the accuracy of the calculated energy partitioning to DF rotation and relative translation are evident. In the experiment, the largest amount of DF rotational excitation measured was 1.4 kcal mol^{-1} (at E_{coll} = 8.37 kcal mol^{-1}), which is notably smaller than the calculated results irrespective of the way trajectories are analyzed. In addition, the largest average final relative translational energy measured was 9.8 kcal mol^{-1} (at E_{coll} = 8.37 kcal mol^{-1}), also smaller than the calculated results. These results clearly point out inaccuracies in the calculations, which originate from the potential-energy surface, the quasiclassical-trajectory method, or more likely a combination of both. Some of the errors in the quasiclassical trajectories might emerge from excessive leakage of the energy of reagent normal modes that should largely be adiabatic into the reaction coordinate. In an attempt to quantify the possible errors introduced by excessive zero-point-energy leakage, we have performed trajectory calculations at E_{coll} = 5.37 kcal mol^{-1} with varying degrees of initial vibrational excitation in CD_4. Calculations with one-half or one-quarter of the initial CD_4 vibrational energy used in the calculations of Table 4 indicate a correlation between initial CD_4 vibration and final DF and CD_3 internal energy. However, the amount of energy released into product relative translation is unaffected by the amount of initial vibrational energy in CD_4, suggesting that the overestimation of experiments by our calculations in this property discussed before is likely a weakness of the SRP-MSINDO Hamiltonian derived in this work.

In addition to energy partitioning in products, the CD_3-(0000,N≈4) state-specific measurements provided information about the angular distributions. In particular, DF vibrational state-resolved angular distributions clearly showed an evolution from backward scattering to sideways and forward scattering with increasing vibrational excitation in DF.[1] In Figure 7a, we show DF vibrational-specific angular distributions obtained in the F + CD_4 → DF + CD_3 reaction at E_{coll} = 5.37 kcal mol^{-1}. The calculations replicate the trend that highly vibrationally excited DF has a larger propensity than vibrationally colder DF to scatter in the forward direction. This is an important result,

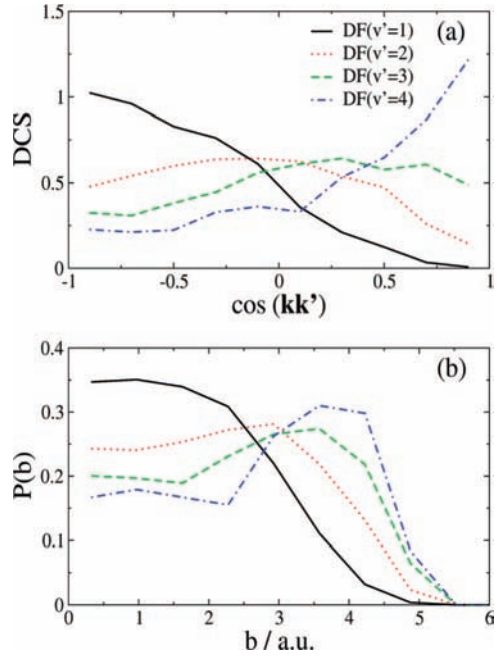

Figure 7. Calculated DF vibrational state-specific angular distributions in terms of differential cross sections (a) and opacity functions (b) for the F + CD_4 → DF + CD_3 reaction at E_{coll} = 5.37 kcal mol^{-1}. The distributions are normalized for area. Absolute cross sections for the DF(v') = 1, 2, 3, and 4 states are (in au) 10.4, 21.4, 14.3, and 1.6, respectively.

as the experiments speculated that forward scattering for DF(v'=4) might herald the appearance of a reactive resonance. The presence of a backward → forward trend with increasing DF excitation in our classical calculations indicates that a reactive resonance does not seem necessary to obtain this trend. Instead, the DF vibrational state-specific opacity functions in Figure 7b show that the trend can be partially explained by the preference of collisions at longer impact parameters to form vibrationally excited DF. These reactions at long impact parameters also provide more forward scattering, as F + alkane reactions are dominated by a direct reaction mechanism.

In summary, comparisons between the predictions of the SRP-MSINDO Hamiltonian derived in the work and experimental results on the F + CH_4, F + CD_4, and F + C_2H_6 reactions reveal that the Hamiltonian captures the broader aspects of the dynamics, including the amount of vibrational energy partitioned into the newly formed bond and angular distributions. Even though the agreement with experiment is not quantitative in some properties, all of the experimental trends are satisfactorily reproduced by the calculations. In the following, we present a comparative study between the dynamics of the F + CH_4, F + C_2H_6, F + C_3H_8, and F + i-C_4H_{10} reactions with the goal of identifying how the size of the alkane molecule and the site of abstraction influence the reaction dynamics.

B. Comparative Study of F + Alkane Reactions. Figure 8a shows the HF vibrational distributions of all the channels of all 4 chemical reactions investigated in this work at E_{coll} = 3.2 kcal mol^{-1}. Leaving the F + CH_4 reaction aside, the trend for the rest of the reactions at primary abstraction sites is that HF vibrational excitation decreases with increasing size of the reagent alkane molecule. Since the exothermicity of the primary abstraction reaction is very similar for all F + alkane reactions studied here except F + CH_4, the conclusion offered by these results is that the size of the alkane molecule helps channel energy in modes other than HF vibration. Comparing the HF vibrational distributions for abstraction at primary vs. secondary

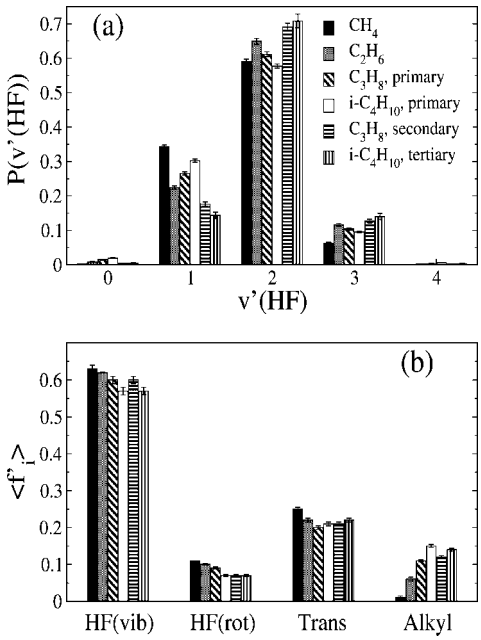

Figure 8. Calculated HF vibrational state distributions (a) and average fractions of available energy in products (b) for various F + alkane reactions at E_{coll} = 3.2 kcal mol^{-1}. The average fractions of alkyl internal energy and HF vibrational energy in part b are calculated from the corresponding zero-point energy levels.

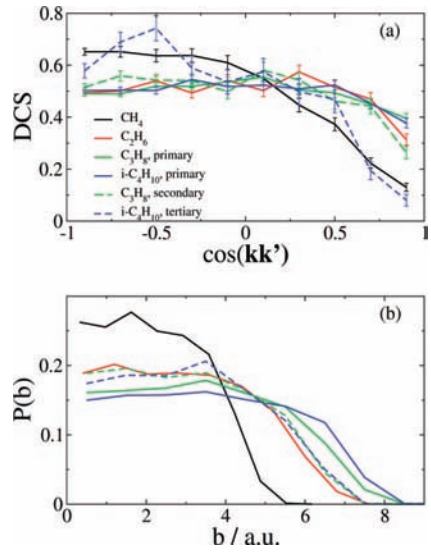

Figure 9. Calculated angular distributions expressed in terms of differential cross sections (a) and opacity functions (b) for various F + alkane reactions at E_{coll} = 3.2 kcal mol^{-1}. The distributions are normalized for area. Absolute cross sections for the F + CH_4, C_2H_6, C_3H_8, and *i*-C_4H_{10} reactions are (in au) 50.9, 96.2, 120.7, and 142.0, respectively.

and tertiary sites reveals that energy release to HF vibration increases along the primary → secondary → tertiary sequence. This result bodes well with the corresponding exothermicities.

To gain further insight into these trends, we show in Figure 8b fractions of available energy into various products degrees of freedom for all of the channels in all of the reactions studied at E_{coll} = 3.2 kcal mol^{-1}. The figure shows that the HF vibration is the preferred mode for energy deposition in products, followed by relative translation. In comparison, partitioning to HF rotation and internal alkyl energy is relatively small. Examination of the average fractions of energy in products for the primary channels of all reactions indicates a general trend to decrease the fraction of energy going into HF vibration, rotation, and translation with the size of the reagent alkane molecule. Consequently, the fractions of energy going into the alkyl fragment rise rapidly for larger alkane molecules. This result suggests that the modes of the alkyl moiety that do not participate directly in the bond breakage/formation process governing F + alkane reactivity are not entirely orthogonal to the reaction coordinate. The origin of the fact that energy partitioning into the alkyl degrees of freedom is enhanced for reactions involving larger alkanes is likely the rapid growth of low-energy normal modes. These large-amplitude vibrational modes of the forming alkyl moiety can effectively couple to the reaction coordinate and absorb energy released in the reactive process. Comparison of energy partitioning into the alkyl product between primary and secondary sites in the F + C_3H_8 reaction and primary and tertiary sites in the F + *i*-C_4H_{10} reaction shows a relative insensitivity of the fractions to the abstraction site. Therefore, the fact that the HF vibrational distributions exhibited in Figure 8a are more excited for secondary and tertiary sites than for primary sites is primarily driven by the larger exothermicity of the former sites.

Finally, we present the angular distributions of the various reactions and channels at E_{coll} = 3.2 kcal mol^{-1} in Figure 9a, and the corresponding opacity functions in Figure 9b. The angular distributions show a larger flux in the backward hemisphere than in the forward hemisphere. This result, in combination with the large reaction probabilities at low impact parameters in Figure 9b, suggests that a direct rebound-like mechanism in which the HF product travels in a direction opposite to that followed by the F atom is more probable than a mechanism in which the F atom abstracts a hydrogen atom as it flies past the molecules without significantly changing its direction of travel. Leaving the results of the F + methane reaction aside, we see that the angular distributions for all of the reactions at primary sites essentially overlap. This result suggests that the reaction mechanism is largely the same for all of these abstraction reactions. A more interesting result emerges when comparing the angular distributions of the primary and secondary channels in the F + C_3H_8 reaction; reaction at secondary sites results in slightly more backward angular distributions than at primary sites. This trend is exaggerated when comparing primary and tertiary sites in the F + *i*-C_4H_{10} reaction, where the angular distribution for tertiary sites is clearly more backward than that of the primary sites. The origin of such a result seems to be tied to the location of the secondary and tertiary sites of the propane and isobutane molecules with respect to primary sites. Primary sites are more removed from the center of mass than secondary or tertiary sites, thereby enabling reactions at longer impact parameters. In these more peripheral reactions on primary sites, the fluorine atom can abstract a primary hydrogen atom without largely changing its momentum, which enhances forward scattering. This mechanism is popularly known as stripping dynamics. The presence of enhanced stripping dynamics in abstractions at primary sites due to a more peripheral reaction is reinforced by the opacity functions in Figure 9b. In that figure, one can see that reactions at primary sites in F + C_3H_8 and F + *i*-C_4H_{10} collisions do indeed take place at longer impact parameters than in the corresponding secondary and tertiary sites. The figure can also be used to provide an estimate of the effective size of the alkane molecules used in this work. In effect, comparison of the maximum impact parameters leading to reaction for all the primary abstraction sites shows the expected trend that the effective molecular size increases in the methane → ethane → propane → isobutane sequence.

IV. Concluding Remarks

We have used ab initio calculations to map the potential-energy surface of the F + CH_4 and F + C_2H_6 reactions in areas predominantly around the minimum-energy reaction path, but also exploring other areas of the PES that are energetically accessible in previously reported experimental studies. Using this ab initio information, we have reparameterized the MSINDO semiempirical Hamiltonian to correct the largest errors of this electronic-structure method in its description of the F + alkane reactions, particularly the sharp overestimation of the exothermicities of the reactions. The empirical parameter set specific to the F + alkane hydrogen abstraction reactions endows the MSINDO Hamiltonian with a good degree of accuracy in comparison with CCSD(T)/aug-cc-pVDZ energies. Except for the shallow intermolecular wells in the reagents and products valleys, the SRP-MSINDO Hamiltonian is shown to outperform the predictions of MP2/aug-cc-pVDZ calculations for the regions of the potential-energy surface covered in our study.

Using this computationally inexpensive SRP-MSINDO Hamiltonian, we have carried out an extensive direct-dynamics quasiclassical trajectory study of the F + methane, ethane, propane, and isobutane reactions. To test the accuracy of the Hamiltonian in dynamics calculations, we have compared a variety of calculated dynamics properties with available experiments, including HF vibrational distributions, energy partitioning in products, and vibrational state-specific angular distributions. The SRP-MSINDO Hamiltonian is seen to reproduce all of the trends found in the experiment, but the agreement with experiment is not always quantitative, particularly in regards to the amount of energy released to HF rotation and relative translation.

Comparison of the dynamics of the hydrogen-abstraction F + alkane reactions studied in this work reveals a number of interesting results. First, HF vibrational distributions of reactions at primary sites become increasingly colder as the size of the reagent alkane molecule increases. This result seems to be tied to the increase in the number of energy modes that larger alkyl molecules can couple to the reaction coordinate, which effectively absorb some of the energy released during reaction. On the other hand, the HF vibrational distributions become increasingly hotter for reactions along the primary → secondary → tertiary abstraction-site sequence. This is a consequence of the increase in exothermicity along that sequence, and not to a difference in the relative energy partitioning in products for the various sites. Analysis of angular distributions and opacity functions helps elucidate the broader aspects of the reaction mechanisms. Reactions at primary sites are more peripheral than those at secondary and tertiary sites, and therefore exhibit less backward scattering than the more central reactions.

A major conclusion of this work is that reparameterization of a semiempirical Hamiltonian is an attractive strategy to enable dynamics studies of relatively large chemical reactions. Our study shows that by using extensive ab initio information of only the smallest members of a family of chemical reactions, one can generate electronic-structure methods that are reasonably accurate for homologous reactions in the family. While the semiempirical Hamiltonians are not appropriate for extremely precise studies in which subchemical accuracy is required in the potential-energy surface, this paper contains evidence that they can capture most of the reaction-dynamics trends. A natural extension of this method will be to study radical + condensed-phase alkanes, which are currently being probed in a number of experiments.

Acknowledgment. This work has been supported by NSF Grant. Nos. CHE-0547543 and AFOSR Grant No. FA9550-06-1-0165. D.T. is a Cottrell Scholar of Research Corporation.

References and Notes

(1) Lin, J. J.; Zhou, J.; Shiu, W.; Liu, K. *Science* **2003**, *300*, 966.
(2) Camden, J. P.; Bechtel, H. A.; Ankeny Brown, D. J.; Martin, M. R.; Zare, R. N.; Hu, W.; Lendvay, G.; Troya, D.; Schatz, G. C. *J. Am. Chem. Soc.* **2005**, *127*, 11898.
(3) Simpson, W. R.; Rakitzis, T. P.; Kandel, S. A.; Orr-Ewing, A. J.; Zare, R. N. *J. Chem. Phys.* **1995**, *103*, 7313.
(4) Harper, W. W.; Nizkorodov, S. A.; Nesbitt, D. J. *J. Chem. Phys.* **2000**, *113*, 3670.
(5) Whitney, E. S.; Zolot, A. M.; McCoy, A. B.; Francisco, J. S.; Nesbitt, D. J. *J. Chem. Phys.* **2005**, *122*, 124310.
(6) Wen, L.; Cunshun, H.; Patel, M.; Wilson, D.; Suits, A. *J. Chem. Phys.* **2006**, *126*, 11102.
(7) Varley, D. F.; Dagdigian, P. J. *J. Phys. Chem.* **1996**, *100*, 4365.
(8) Mielke, S. L.; Peterson, K. A.; Schwenke, D. W.; Garrett, B. C.; Truhlar, D. G.; Michael, J. V.; Su, M.-C.; Sutherland, J. W. *Phys. Rev. Lett.* **2003**, *91*, 063201.
(9) Wang, X.; Dong, W.; Chunlei, X.; Che, L.; Wang, X.; Casavecchia, P.; Yang, X.; Jiang, B.; Xie, D.; Lee, S.-Y.; Zhang, D. H.; Werner, J.-H.; Alexander, M. H. *Science* **2008**, *322*, 573.
(10) Zhang, X.; Braams, B. J.; Bowman, J. M. *J. Chem. Phys.* **2006**, *124*, 021104.
(11) Xie, Z.; Braams, B. J.; Bowman, J. M. *J. Chem. Phys.* **2005**, *122*, 224307.
(12) Bolton, K.; Hase, H. L. In *Modern Methods for Multidimensional Dynamics Computations in Chemistry*; Thompson, D. L., Ed.; World Scientific: Singapore, 1998; p 143.
(13) Bredow, T.; Jug, K. *Theor. Chem. Acc.* **2005**, *113*, 1.
(14) Gonzalez-Lafont, A.; Truong, T. N.; Truhlar, D. G. *J. Phys. Chem.* **1991**, *95*, 4618.
(15) Hu, W.; Lendvay, G.; Troya, D.; Schatz, G. C.; Camden, J. P.; Bechtel, H. A.; Brown, D. J. A.; Martin, M. R.; Zare, R. N. *J. Phys. Chem. A* **2006**, *110*, 3017.
(16) Peslherbe, G. H.; Hase, W. L. *J. Chem. Phys.* **1996**, *104*, 7882.
(17) Yan, T.; Doubleday, C.; Hase, W. L. *J. Phys. Chem. A* **2004**, *108*, 9863.
(18) Troya, D.; Garcia-Molina, E. *J. Phys. Chem. A* **2005**, *109*, 3015.
(19) Troya, D. *J. Phys. Chem. A* **2005**, *109*, 5814.
(20) Troya, D. *J. Chem. Phys.* **2005**, *123*, 214305.
(21) Troya, D.; Weiss, P. J. E. *J. Chem. Phys.* **2006**, *124*, 74313.
(22) Layfield, J. P.; Owens, M. D.; Troya, D. *J. Chem. Phys.* **2008**, *128*, 194302.
(23) Layfield, J. P.; Troya, D. *Chem. Phys. Lett.* **2008**, *467*, 243.
(24) Parker, J. H.; Pimentel, G. C. *J. Chem. Phys.* **1969**, *51*, 91.
(25) Sugawara, K.-i.; Ito, F.; Nakanaga, T.; Takeo, H.; Matsumura, C. *J. Chem. Phys.* **1990**, *92*, 5328.
(26) Shiu, W.; Lin, J. J.; Liu, K.; Wu, M.; Parker, D. H. *J. Chem. Phys.* **2004**, *120*, 117.
(27) Harper, W. W.; Nizkorodov, S. A.; Nesbitt, D. J. *Chem. Phys. Lett.* **2001**, *335*, 381.
(28) Zhou, J.; Lin, J. J.; Shiu, W.; Pu, S.-C.; Liu, K. *J. Chem. Phys.* **2003**, *119*, 2538.
(29) Shiu, W.; Lin, J. J.; Liu, K.; Wu, M.; Parker, D. H. *J. Chem. Phys.* **2004**, *120*, 117.
(30) Espinosa-Garcia, J. *J. Phys. Chem. A* **2007**, *111*, 3497.
(31) Troya, D.; Millan, J.; Banos, I.; Gonzalez, M. *J. Chem. Phys.* **2004**, *120*, 5181.
(32) Castillo, J. F.; Aoiz, F. J.; Banares, L.; Martinez-Nunez, E.; Fernandez-Ramos, A.; Vazquez, S. *J. Phys. Chem. A* **2005**, *109*, 8459.
(33) Frisch, M. J.; Trucks, G. W.; Schlegel, H. B.; Scuseria, G. E.; Robb, M. A.; Cheeseman, J. R.; Montgomery J. A., Jr.; Vreven, T.; Kudin, K. N.; Burant, J. C.; Millam, J. M.; Iyengar, S. S.; Tomasi, J.; Barone, V.; Mennucci, B.; Cossi, M.; Scalmani, G.; Rega, N.; Petersson, G. A.; Nakatsuji, H.; Hada, M.; Ehara, M.; Toyota, K.; Fukuda, R.; Hasegawa, J.; Ishida, M.; Nakajima, T.; Honda, Y.; Kitao, O.; Nakai, H.; Klene, M.; Li, X.; Knox, J. E.; Hratchian, H. P.; Cross, J. B.; Bakken, V.; Adamo, C.; Jaramillo, J.; Gomperts, R.; Stratmann, R. E.; Yazyev, O.; Austin, A. J.; Cammi, R.; Pomelli, C.; Ochterski, J. W.; Ayala, P. Y.; Morokuma, K.; Voth, G. A.; Salvador, P.; Dannenberg, J. J.; Zakrzewski, V. G.; Dapprich, S.; Daniels, A. D.; Strain, M. C.; Farkas, O.; Malick, D. K.; Rabuck, A. D.; Raghavachari, K.; Foresman, J. B.; Ortiz, J. V.; Cui, Q.; Baboul, A. G.; Clifford, S.; Cioslowski, J.; Stefanov, B. B.; Liu, G.; Liashenko, A.; Piskorz, P.; Komaromi, I.; Martin, R. L.; Fox, D. J.; Keith, T.; Al.Laham, M. A.; Peng, C. Y.; Nanayakkara, A.; Challacombe, M.; Gill, P. M. W.; Johnson, B.; Chen, W.; Wong, M. W.; Gonzalez, C.; Pople, J. A. *Gaussian03*; Gaussian, Inc., Wallingford CT, 2004.

(34) Reaction energies calculated from the experimental heats of formation at 298 K reported in http://www.iupac-kinetic.ch.cam.ac.uk.
(35) Reaction energies calculated from the experimental heats of formation at 298 K reported in http://webbook.nist.gov/chemistry.
(36) Troya, D. *J. Phys. Chem. A* **2007**, *111*, 10745.
(37) Ahlswede, B.; Jug, K. *J. Comput. Chem.* **1999**, *20*, 572.
(38) Ahlswede, B.; Jug, K. *J. Comput. Chem.* **1999**, *20*, 563.
(39) Andresen, P.; Luntz, A. C. *J. Chem. Phys.* **1980**, *72*, 5842.
(40) Hammond, G. S. *J. Am. Chem. Soc.* **1955**, *77*, 334.
(41) Hase, H. L.; Duchovic, R. J.; Hu, X.; Komornicki, K. F.; Lim, K.; Lu, D.; Peslherbe, G. H.; Swamy, K. N.; Vande Linde, S. R.; Varandas, A. J. C.; Wang, H.; Wolf, R. J. *Quantum Chem. Prog. Exch. Bull.* **1996**, *16*, 671.
(42) Zhou, J.; Lin, J. J.; Shiu, W.; Liu, K. *J. Chem. Phys.* **2003**, *119*, 4997.

JP810929E